

LLM-Feynman: Leveraging Large Language Models for Universal Scientific Formula and Theory Discovery

Zhilong Song¹, Minggang Ju¹, Chunjin Ren², Qiang Li¹, Chongyi Li¹, Qionghua Zhou^{1,2,*}, and Jinlan Wang^{1,2,*}

¹Key Laboratory of Quantum Materials and Devices of Ministry of Education, School of Physics, Southeast University, Nanjing 21189, China

² Suzhou Laboratory, Suzhou, China

Distilling the underlying principles from data has long propelled scientific breakthroughs. However, conventional data-driven machine learning (ML)—lacking deep, contextual domain knowledge—tend to yield opaque or over-complex models that are challenging to interpret and generalize. Here, we present LLM-Feynman, a framework that leverages the embedded expertise of large language models (LLMs) with systematic optimization to distill concise, interpretable formula from data and domain knowledge. Our framework seamlessly integrates automated feature engineering, LLM-based symbolic regression augmented by self-evaluation and iterative refinement, and formula interpretation via Monte Carlo tree search. Ablation studies show that incorporating domain knowledge and self-evaluation yields more accurate formula at equivalent formula complexity than conventional symbolic regression. Validation on datasets from Feynman physics lectures confirms that LLM-Feynman can rediscover over 90% real physical formulas. Moreover, when applied to four key materials science tasks—from classifying the synthesizability of 2D and perovskite structures to predicting ionic conductivity in lithium solid-state electrolytes and GW bandgaps in 2D materials—LLM-Feynman consistently yields interpretable formula with accuracy exceeding 90% and R^2 values above 0.8. By transcending mere data fitting through the integration of deep domain knowledge, LLM-Feynman establishes a new paradigm for the automated discovery of generalizable scientific formula and theory across disciplines.

Introduction

Distilling universal laws from data constitutes the bedrock of scientific advancement throughout history. In the 16th century, Tycho Brahe's meticulous astronomical observation data¹ laid the groundwork for Johannes Kepler's² formulation of planetary motion laws, which paved the way for Isaac Newton's universal law of gravitation³. Fast forward to the modern era, we have an explosion of observation data across virtually all scientific domains. Data-driven machine learning (ML) has emerged as an essential tool for identifying underlying patterns and driving discovery⁴⁻¹³.

Yet, despite their impressive predictive performance, most ML models function as black boxes that prioritize accuracy over interpretability, thereby limiting their ability to reveal explicit scientific formula¹⁴. In contrast, interpretable ML techniques—such as symbolic regression (SR)—aim to bridge this gap by systematically exploring the space of mathematical expressions to identify formula that minimize prediction error¹⁴⁻¹⁶. In material science, for instance, SR has revealed scientific formulas about Gibbs energy of inorganic crystalline solids¹⁷, tolerance factor of perovskite stability¹⁸, perovskite oxygen evolution reaction activity⁹ and oxide support effects in late-transition metal catalysts¹⁹.

However, a fundamental distinction remains between how machines typically discover “laws” and how scientists like Brahe, Kepler, and Newton operate. While data-driven ML can fit models or formula to datasets, it lacks deep and contextual domain knowledge that human scientists possess. This background knowledge not only accelerates the discovery of accurate formulas but also ensures that any newfound formulas are interpretable and generalize well beyond the specific domain. Thus, even interpretable MLs, such as SR often yield overly complex formula that are challenging to explain and may struggle to generalize beyond their training data²⁰. Consequently, there is a growing need for methods that can effectively combine domain knowledge with the data-driven methods to derive generalizable and interpretable scientific formulas.

The rise of pre-trained large language models (LLMs) like DeepSeek^{21,22},

ChatGPT²³ and LLaMA²⁴, offers unprecedented opportunities to bridge this distinction between machines and human scientists. Trained on vast corpora spanning scientific literature, textbooks, and databases, LLMs internalize rich representations of physics, chemistry, and materials science and revolutionized various research domains²⁵. Taking materials science as an example, LLMs have facilitated predicting material properties²⁶, optimizing experimental workflows²⁷, proposing synthesis strategies for organic molecules²⁸, metal-organic frameworks²⁹ and evaluating the synthesizability of inorganic materials^{30,31}. However, leveraging LLMs for automated scientific formula and theory discovery is nontrivial. While these models excel at memorizing and recombining existing knowledge, their autoregressive nature predisposes them to generate plausible-sounding but physically inconsistent formula^{32,33}. Furthermore, in previous attempts that utilized LLMs to discover formulas from data³⁴, have lacked the domain knowledge embedding and necessary multi-objective optimization to balance accuracy, simplicity, and interpretability.

To address these challenges, we developed LLM-Feynman, a framework that synergizes the scientific reasoning of LLMs with structured optimization to discover generalizable, interpretable scientific formula. The framework consists of three primary modules: automatic data preprocessing and feature engineering, LLM-based symbolic regression with self-evaluation and multi-objective optimization, and formula interpretation leveraging Monte Carlo tree search³⁵ based on LLMs. Comprehensive ablation studies demonstrate that our approach outperforms conventional methods such as sure independence screening and sparsifying operator (SISSO)^{36,37} and PySR³⁸ in accuracy while maintaining equivalent model complexity. Remarkably, using datasets constructed from Feynman's physics lectures, LLM-Feynman successfully rediscovered over 90% of physics formula. We further apply LLM-Feynman to four pivotal problems in materials science—the synthesizability of 2D materials and perovskite structures (classification), as well as the ionic conductivity of lithium solid-state electrolytes and the GW bandgap of 2D materials (regression). In all cases, our framework yields interpretable formula with accuracies exceeding 90% and R^2 values above 0.8 on testing data. Through transcending mere data fitting to

incorporate domain knowledge and multi-objective optimization, LLM-Feynman paves the way for the automated discovery of generalizable scientific formula across domains.

2. Results and discussion

2.1. LLM-Feynman framework

In the first module of LLM-Feynman, the data preprocessing and feature engineering module assumes the input data includes features X (dimension $m \times n$, where n is the number of data points and m is the number of features), target values y (dimension $1 \times n$), along with the physical meanings and dimensions of both the features and the target. LLM-Feynman automatically preprocesses the input data by removing missing values and optionally normalizing the features. Importantly, this module incorporates tailored feature engineering for material science problems. Based on the material compositions and structures, we developed three automated feature computational schemes (Figure S1): i) Feature selection via mutual information: A set of initial features X_{ini} is computed using the integrated Automatminer^{39,40} framework. Mutual information is computed between features and the target, as well as among features. Informative features are retained, while redundant ones are removed, yielding the final set X_{final} . ii) LLM-recommended feature matching: The LLM recommends a set of feature names (template in Figure S2), which are subsequently matched in the Matminer³⁹ library (template in Figure S3). Matminer is then used to compute the corresponding feature values. iii) Iterative feature refinement: Building on the second scheme, if the iterative LLM-based formula discovery fails to reduce error over 50 generations, the LLM suggests a new set of features (template in Figure S4). These features are similarly computed using Matminer and merged with the existing feature set. All features derived from these schemes are optionally accompanied by automatically generated physical meanings and dimensions using the LLM. This tailored feature engineering pipeline ensures the discovery of high-quality features, facilitating accurate and interpretable formula generation for diverse tasks in material science.

The second module integrates the feature and target data, along with their physical

meanings and dimensions, into a structured prompt (template provided in Figure S5). Using this prompt, the LLM generates N initial formulas in the form of Python functions. This process is iterative: if fewer than N formulas are generated, the LLM continues to produce additional formulas until the desired number is reached. These formulas are required to exhibit high accuracy while also possessing clear physical and chemical interpretability. Accuracy is quantitatively assessed using metrics such as accuracy, MAE and R^2 . However, interpretability is more challenging to quantify. While lower formula complexity (C) can improve interpretability, it does not necessarily ensure clear physical or chemical meaning. To address this, we leverage the LLM's extensive scientific knowledge to perform a self-evaluation of the interpretability of formulas, assigning a score S (ranging from 0 to 1, template in Figure S6). Next, the Python function formatted text of these formulas is parsed to calculate their error (MAE, R^2 for regression and accuracy, precision, recall, F_1 score, cross-entropy for classification), which is combined with their complexity C and interpretability score S to construct a loss function:

$$L = \alpha N(E) + \beta N(C) + \gamma S$$

Here, N denotes normalization, and the adjustable coefficients α , β , and γ (defaulting to 1) indicate equal weighting of accuracy, complexity, and interpretability. Once the initial formulas are scored with the loss function, the top I formulas (default: 30) are selected. Their mathematical representations, associated loss values, and corresponding data (features, targets, physical meanings, and dimensions) are incorporated into prompts (template in Figure S7) to iteratively guide the LLM in generating J new formulas (default: 10) in each iteration. These new formulas are then self-evaluated and scored using the above loss function. After the specified number (default: 500) of iterations is completed, all formulas are consolidated for Pareto frontier analysis, enabling the identification of formulas that balance high accuracy and simplicity.

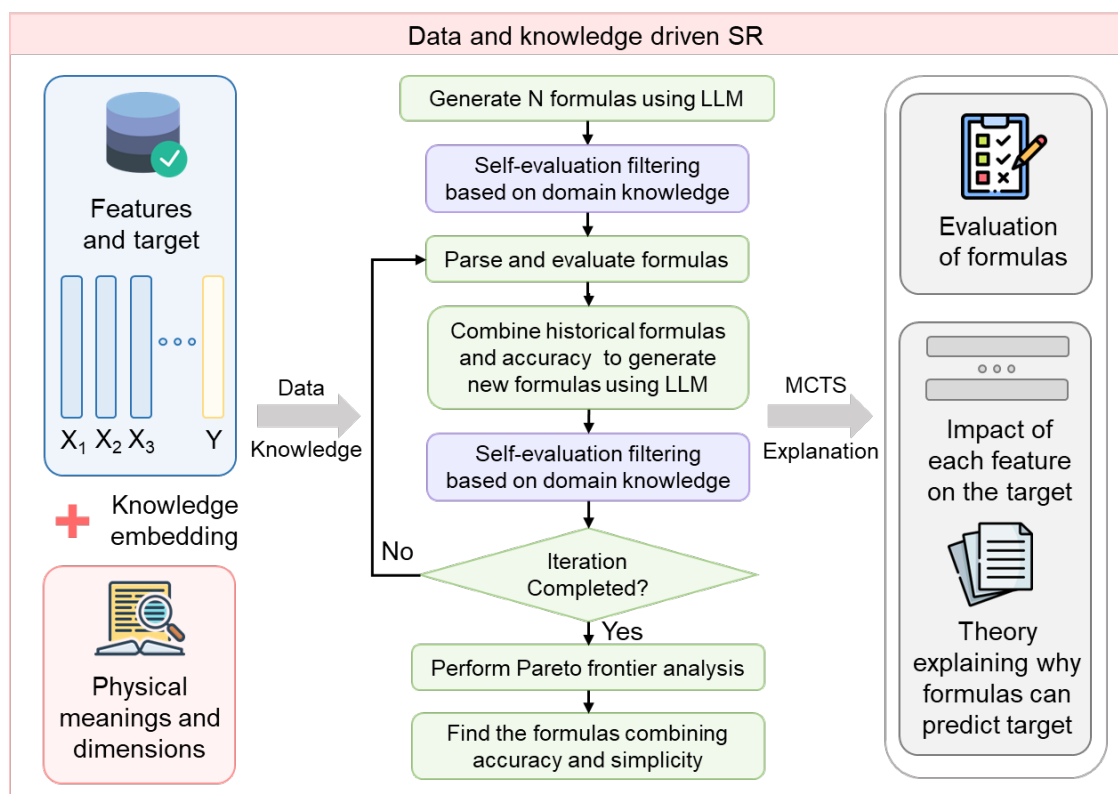


Figure 1. Flowchart of the LLM-Feynman framework. The input consists of data, meaning, and dimensionality of features and targets. Formula are obtained through LLM-based iterative optimization and self-evaluating symbolic regression, followed by deriving interpretative theories using an LLM-based MCTS framework.

The third module of the LLM-Feynman framework integrates Monte Carlo Tree Search (MCTS) with an LLM to systematically interpret and refine the physical and chemical meanings of formula (Figure S7). In this approach, each node in the search tree represents an interpretive idea generated by the LLM, with its score determined by the Upper Confidence Bound (UCB) (details in the Methods section). The LLM evaluates the clarity, scientific relevance, and coherence of generated hypotheses, updating node scores accordingly. By iteratively exploring and refining candidate explanations, MCTS balances the trade-off between exploring novel ideas and prioritizing high-quality interpretations. This synergy between LLM-driven knowledge and MCTS optimization enables efficient navigation of the interpretative space, leading to explanations that are both scientifically meaningful and physically or chemically consistent. Further details are provided in Methods and Supplementary Note S1 and Figure S8-11. Taking the formula μ/t for perovskite OER activity as an example, Figure

S12 illustrates a poor explanation, which receives a self-evaluation score of -72 from the LLM. The primary issue is that it fails to address the core prompt requirement—providing a physical model or theoretical basis for the observed strong linear correlation between μ/t and overpotential. Instead, it merely defines the terms involved, which, while informative, does not constitute a complete scientific explanation (Figure S13). In contrast, the explanation refined through MCTS optimization effectively resolves these shortcomings, achieving a significantly improved self-evaluation score of 65 (Figure S14).

2.2. Performance of LLM-Feynman

We conducted ablation experiments on the LLM-Feynman framework using DFT calculation data for single-atom catalysts (SACs). The dataset comprises adsorption energies ΔE of intermediates (H, OH, CO, and N) on SACs, where the support metals are Cu and Ag, and the guest elements include W, Mo, Os, Ru, Ir, Rh, Pt, and Pd. Six features were computed for these SACs, including the coordination number of the guest site, the valence electron counts of the guest and support metals, their electronegativities, and atomic radii. A detailed feature list is provided in Table S1.

LLM-Feynman was then employed to discover formula capable of predicting the adsorption energies (ΔE_{CO} , ΔE_{OH} , ΔE_{H} , and ΔE_{N}) based on these six features under three modes: (I) Data-driven: feature meanings and dimensions were not provided, and no self-evaluation interpretability score (S) was used during formula discovery; (II) Data-driven and knowledge-driven: building on Mode I, feature meanings and dimensions were provided; (III) Full LLM-Feynman framework: incorporating knowledge embedding and self-evaluation. We tested three LLMs—Falcon-Mamba-7B⁴¹, ChemLLM-20B⁴², and LLaMA3-8B⁴³—comparing their performance against existing data-driven symbolic regression methods, SISSO³⁷ and PySR³⁸. For each approach, we evaluated the average R^2 , MAE, and formula complexity of the top 1,000 formula identified for ΔE_{CO} , ΔE_{OH} , ΔE_{H} , and ΔE_{N} .

As shown in Figure 2a and b, the Data-driven LLM-Feynman framework slightly outperformed SISSO and PySR in terms of average R^2 and MAE, although it exhibited higher average formula complexity. Among the tested LLMs, Falcon-Mamba-7B

showed a significant performance gap compared to LLaMA3-8B and ChemLLM and was excluded from subsequent tests. Upon embedding feature knowledge, the LLM-Feynman achieved a slight reduction in accuracy but exhibited a marked decrease in formula complexity, suggesting improved interpretability. When further incorporating self-evaluation, the full LLM-Feynman framework demonstrated a significant accuracy improvement over SISSO and PySR without increasing formula complexity. Notably, the performance of ChemLLM surpassed that of LLaMA3 in every test, likely due to its specialized fine-tuning on data from the field of chemical materials, which endows it with more comprehensive chemical knowledge compared to LLaMA3. This ablation experiment demonstrates the effectiveness of knowledge embedding and self-evaluation in leveraging the scientific reasoning capabilities of LLMs, thereby enhancing the accuracy and simplicity of the derived formula.

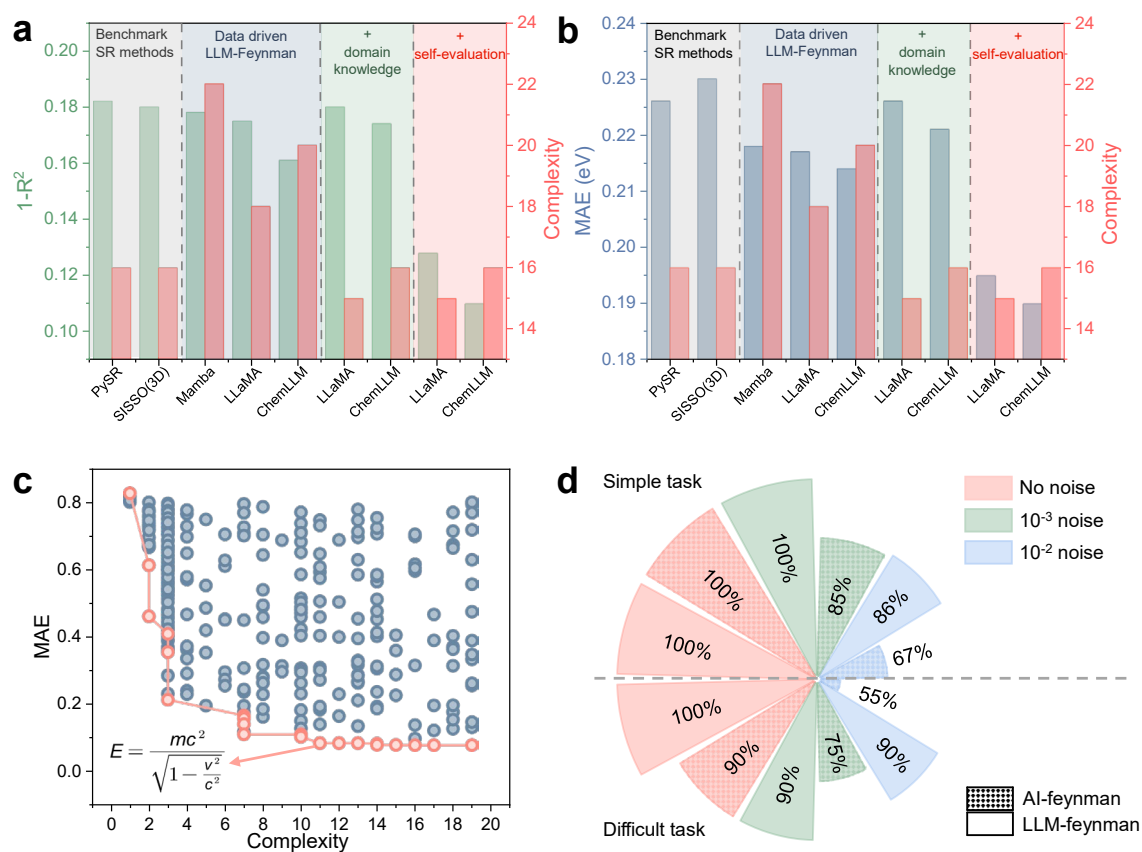


Figure 2. Performance of the LLM-Feynman framework. Comparison of (a) $1-R^2$ vs. complexity and (b) MAE vs. complexity among purely data-driven LLM-Feynman, LLM-Feynman with domain knowledge, LLM-Feynman further incorporating self-evaluation, and traditional SR methods SISSO and SR. (c) Pareto frontier obtained by LLM-Feynman in deriving the mass-energy equation in special relativity. (d) Success rate comparison between

LLM-Feynman and AI-Feynman in discovering 100 simple formulas (simple task) and 30 complex formulas (difficult task) from Feynman’s Lectures on Physics under different noise levels.

In the previous ablation experiments, there were no correct reference formula to evaluate the results. To further validate whether the LLM-Feynman framework can discover formula consistent with physical laws, we collected 100 basic formulas from the Feynman Lectures on Physics as a simple task and 20 more complex formula as a difficult task. We then conducted comparative tests between a conventional SR method with physical constrains—AI-Feynman⁴⁴ and LLM-Feynman based on ChemLLM. For both tasks, the feature and target data were generated from the respective formula, with values normalized to the range [0, 1] and Gaussian noise added at levels of 0, 10^{-3} , and 10^{-2} . For the LLM-Feynman framework, the output is a Pareto frontier, and a formula is considered correctly identified if it appears on the Pareto frontier. Figure 2c presents an example of the Pareto frontier obtained using LLM-Feynman to discover the mass-energy formula in special relativity (with 10^{-2} data noise). The correct formula is positioned at the lower left corner of the Pareto frontier, balancing both accuracy and simplicity.

As shown in Figure 2d, both LLM-Feynman and AI-Feynman successfully identified all formula when no noise was added in the simple task. Under 10^{-3} and 10^{-2} noise, however, LLM-Feynman maintained success rates of 100% and 86%, respectively, significantly outperforming AI-Feynman, which achieved 85% and 67%. The performance gap widened in the difficult task: under 10^{-2} noise, LLM-Feynman still achieves a 90% success rate, whereas AI-Feynman dropped to 55%. These results highlight the advantages of LLM-Feynman, which can be attributed to the extensive physical and chemical knowledge embedded in pre-trained LLMs, enabling it to better handle complex formula and noisy data while maintaining high accuracy.

2.3. Application in the synthesizability of 2D materials

After validating the high accuracy, interpretability, and robustness of the LLM-Feynman framework in discovering physically meaningful and simplified formula, we applied it to explore formula for predicting the synthesizability of 2D materials. The synthesizability of 2D materials is critical due to their transformative applications in

fields such as electronics, energy storage, catalysis, and optoelectronics. While theoretical studies, supported by databases like Computational 2D Materials Database (C2DB)⁴⁵, Materials Cloud^{46,47}, and 2DMatPedia⁴⁸, predict the existence of 16789 potential 2D materials, only around 100 have been experimentally synthesized. This substantial gap underscores the challenge of experimentally realizing theoretically predicted materials and highlights the need for a formula capable of predicting synthesizability based on simple features of 2D materials.

To achieve this, we first need to construct a balanced database containing both synthesizable positive samples and non-synthesizable 2D materials negative samples (Figure 3a). However, no experimental database for 2D materials is currently available. Thus, we used PyPaperBot to download 360 experimental papers on 2D materials and employed an LLM to parse these papers, extracting compositions confirmed to have been successfully synthesized. After manual verification, we identified a total of 170 2D material compositions (Table S2). Next, we need to obtain the structures of these materials. Since experimental papers typically do not provide structure files (e.g., CIF or POSCAR formats), we first searched the Inorganic Crystal Structure Database (ICSD) experimental database⁴⁹ for layered structures corresponding to these compositions. After removing duplicates, we used clustering algorithms to extract single-layer structures. For compositions with multiple candidate single-layer structures, we performed DFT calculations and selected the one with the lowest energy. For compositions without layered structures in the ICSD database, we sourced 2D structures with the lowest decomposition and exfoliation energies from theoretical databases C2DB, Materials Cloud and 2DMatPedia. Compositions for which neither approach was successful were excluded. Ultimately, we obtained 151 experimentally synthesized 2D materials structures as positive samples.

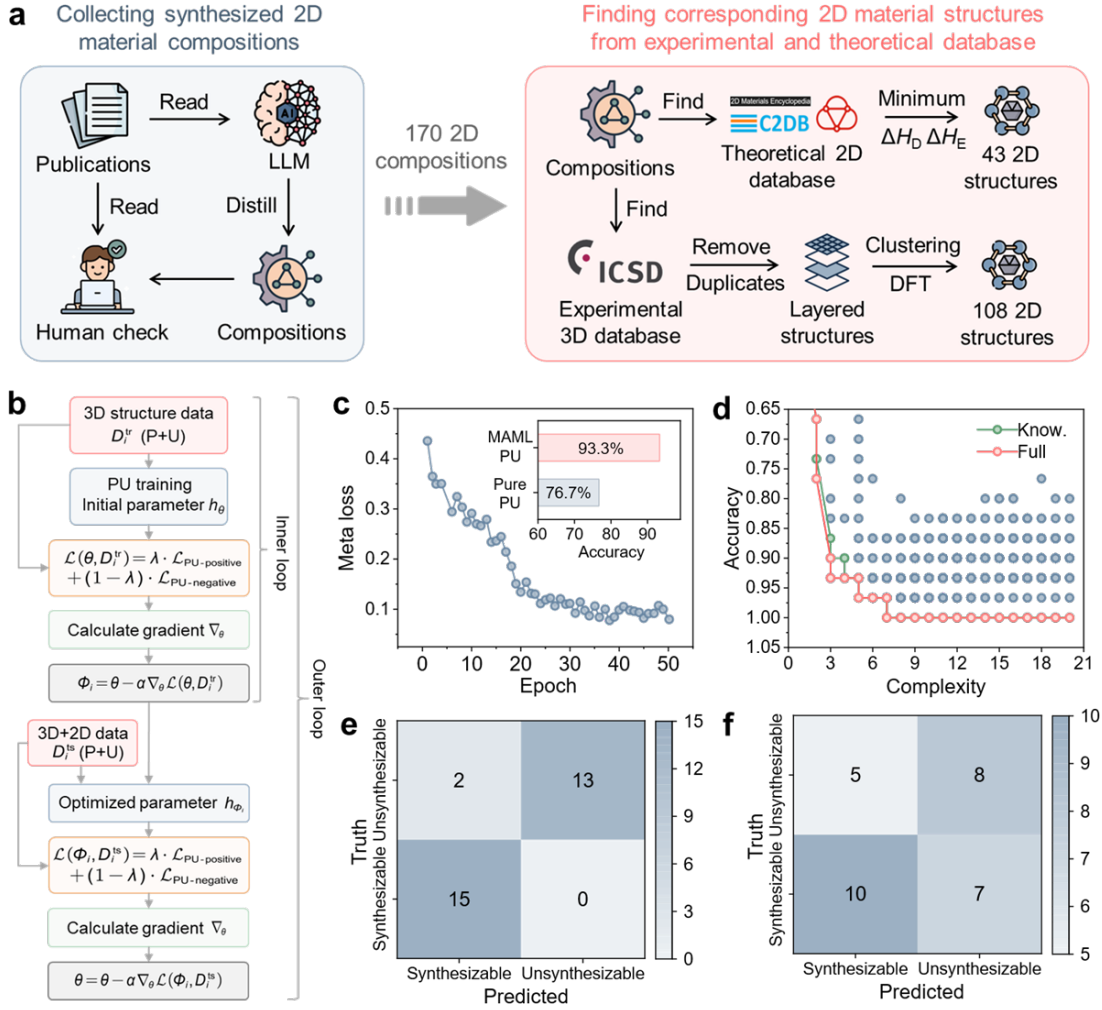


Figure 3. Performance of LLM-Feynman in the synthesizability of 2D materials. **(a)** Workflow for constructing a database of experimentally synthesized 2D material structures, including LLM-based and manually verified extraction of experimentally synthesized 2D material compositions, as well as structure extraction from experimental and theoretical databases. **(b)** Training process of the PU learning combined with the MAML framework for identifying non-synthesizable 2D material structures. **(c)** Loss reduction during the training of the PU learning combined with the MAML framework. The inset compares the classification performance of the PU learning model with and without MAML. **(d)** Pareto frontier obtained by LLM-Feynman in exploring the formula for the synthesizability of 2D materials. **(e)** Confusion matrix of the best formula discovered by LLM-Feynman. **(f)** Confusion matrix of E_{hull} for classifying the synthesizability of 2D materials.

The second step involves constructing an equal number of non-synthesizable 2D materials as negative samples. However, unlike standard binary classification, where both positive and negative labels are available, synthesizability prediction lacks confirmed non-synthesizable materials, leaving only positive and unlabeled samples. Thus, positive-unlabeled (PU) learning, a method commonly used in synthesizability classification for 3D crystal structures, was employed in this application. The process begins by treating the experimentally synthesized 2D materials as the positive class.

Theoretical 2D materials from C2DB and Materials Cloud, excluding those confirmed as synthesizable, form the unlabeled set. A PU learning model⁵⁰ based on Crystal Graph Convolutional Neural Networks (CGCNN)⁵¹ was then trained in two stages. First, an initial classifier is trained using positive samples and a subset of unlabeled data assumed to contain a high proportion of negatives. Second, the classifier iteratively refines its decision boundary by reassigning high-confidence negatives within the unlabeled set. By leveraging this iterative self-learning process, PU learning can identify non-synthesizable 2D materials (*i.e.*, 2D structures with very low model output values) without requiring explicit negative labels, ultimately constructing a balanced training dataset across elements and symmetry for synthesizability prediction (Figure S15).

However, the classification accuracy of the final PU learning model was only 76.7%, meaning some 2D structures with very low model output values might still be synthesizable. To address this, we integrated a meta-learning approach, MAML (Model-Agnostic Meta-Learning)⁵², into the PU learning framework to improve accuracy in identifying non-synthesizable 2D materials. As shown in Figure 3b, MAML optimizes the model's ability to adapt quickly to new tasks, including two steps: I) Inner Loop: The model is trained on 3D material structures data, learning task-specific parameters by iteratively adjusting based on the current dataset. II) Outer Loop: These task-specific parameters are then fine-tuned using combined 3D and 2D structures data, ensuring the model learns generalizable parameters that can perform well across tasks. (details in Supplementary Note S2) By repeatedly alternating between these steps 50 times, MAML effectively addresses the limitations of PU learning alone and significantly enhances classification accuracy to 93.3% (Figure 3c).

After obtaining a high-accuracy PU learning model, we applied it to predict all 2D structures in the C2DB, Materials Cloud and 2D MatPedia databases. From these predictions, the 150 2D structures with the lowest output scores were selected as non-synthesizable materials, creating a balanced dataset for 2D material synthesizability (positive: negative = 151:150). The dataset was then split into training and testing sets at an 8:2 ratio for running the LLM-Feynman framework. Using the first automated feature engineering scheme, the Automatminer library computed 1,200 structural and compositional features. After screening with the mutual information method, 52 features were retained to explore formulas, which were analyzed through Pareto frontier optimization based on four performance metrics on testing sets—accuracy, precision, recall, and F1 score—as well as formula complexity (Figure S16-18). As shown in

Figure 3d, the green line for LLM-Feynman without self-evaluation shows lower formula accuracy than the red line for LLM-Feynman with self-evaluation at the same complexity. This highlights the role of self-evaluation in leveraging the scientific knowledge of LLMs more effectively, thereby enhancing formula performance.

From the four Pareto frontiers, two formulas from the lower-left corner were selected for each, resulting in six non-redundant formula that balance accuracy and complexity (Table S3-4). Among these, the following formula, appearing on the Pareto frontier of accuracy vs. complexity (Figure 3d), achieved the highest self-evaluation interpretability scores:

$$\text{MeanUnfilled} - \text{Hal} \times \text{RangeRow} - E_{\text{Hull}}$$

where MeanUnfilled, Hal, RangeRow, and E_{Hull} represent the average number of unfilled p -electrons in non-metal elements, the presence of halogen elements, the range of periodic table rows of the elements, and the convex hull energy of formation enthalpy, respectively. We then compared this formula with a classification approach that uses only E_{hull} to distinguish synthesizable ($E_{\text{hull}} \leq 0.2$ eV/atom) and non-synthesizable 2D materials ($E_{\text{hull}} > 0.2$ eV/atom). Only two synthesizable 2D materials were misclassified using those formula on the test set (Figure 3e). The accuracy, precision, recall, and F_1 score on the test set reach 0.93, 0.88, 1.00, and 0.94, respectively, significantly outperforming the E_{hull} -only classification (Figure 3f and Table 1). This demonstrates that relying solely on thermodynamic E_{hull} to evaluate 2D material synthesizability is insufficient.

Table 1. Performance of classification formula for the synthesizability of 2D materials and perovskites on the test set.

Formula	Accuracy	Precision	Recall	F_1 score	Complexity
2D material	0.93	0.88	1.00	0.94	7
2D material (E_{hull})	0.60	0.61	0.53	0.57	1
Perovskite	1.00	1.00	1.00	1.00	12

The MCTS-based LLM explanation of the formula revealed that it integrates three key factors to comprehensively evaluate the 2D material synthesizability: electronic structure features, elemental types and composition, and thermodynamic stability. Factors enhancing synthesizability include: I) High average unfilled p -electron count: Promotes covalent bond formation and improves structural stability. II) Low E_{hull} values: Indicates higher thermodynamic stability, making experimental synthesis more feasible.

Conversely, factors reducing synthesizability include: I) Presence of halogen elements: Increases chemical reaction complexity and uncertainty, lowering stability. II) High range of periodic table rows: large differences in atomic size and properties lead to lattice mismatch and structural stress. The full explanation is shown in Supplementary Note S3.

2.4. Applications in the synthesizability of perovskites, conductivity of solid-state electrolyte and GW bandgap of 2D materials

To further validate the reliability of LLM-Feynman in practical applications, we applied it to another classification task. Perovskites have attracted significant attention in recent years due to their wide-ranging applications in optoelectronics, photovoltaics, and catalysis. Understanding their synthesizability is crucial for advancing the discovery of new perovskites. Thus, we aimed to identify formula for the synthesizability of perovskites. To construct a balanced dataset, we collected 3,317 experimentally synthesized perovskite structures from the Materials Project⁵³ database. Using the same CGCNN-based PU learning approach in the previous application, we generated an equal number of 3,317 negative samples from Materials Project and Open Quantum Materials Database (OQMD)⁵⁴. In this case, MAML was not incorporated, as the trained PU learning model already achieved 95% accuracy. Next, LLM-Feynman applied Automatminer and mutual information filtering to extract 141 compositional and structural features, which were used to identify formula through Pareto frontier analysis. Four Pareto frontiers were generated, corresponding to accuracy, precision, recall, and F₁ score vs. complexity. Among them, the following formula achieved the highest LLM self-evaluation interpretability score on the accuracy vs. complexity frontier (Figure 4a):

$$\text{crystal_sys_sum} + \frac{\text{NpValence_mode}}{(\text{NUnfilled_mean} + \text{Row_avg_dev})^3}$$

where `crystal_sys_sum`, `NpValence_mode`, `NUnfilled_mean`, and `Row_avg_dev` represent whether the structure belongs to the cubic, tetragonal, or trigonal crystal system; the mode of the *p*-valence electron count across all elements; the mean number of unfilled valence orbitals across all elements; and the average deviation of the periodic table row numbers of all elements, respectively. This formula achieved outstanding

performance (1.00 accuracy, precision, recall, and F_1 score) on the test set (Table 1 and Figure 4b). According to the MCTS-based explanation framework (details in Supplementary Note S4), this formula evaluates perovskite synthesizability by integrating structural and electronic factors. Structural components include binary indicators (0/1) for cubic, tetragonal, or trigonal crystal systems, where their sum reflects structural stability as these symmetric arrangements favor ion compatibility. Electronic parameters comprise: I) mode_NpValence, indicating bonding synergy; II) mean NUnfilled, balancing bond potential vs. instability risks; III) avg_dev_Row, assessing atomic size/energy alignment. The cubed denominator amplifies penalties for high unfilled orbitals or large period mismatches, while the numerator emphasizes electronic harmony. Higher values correlate with favorable crystal symmetry, strong bonding compatibility, and minimized destabilizing factors, enabling precise synthesizability prediction.

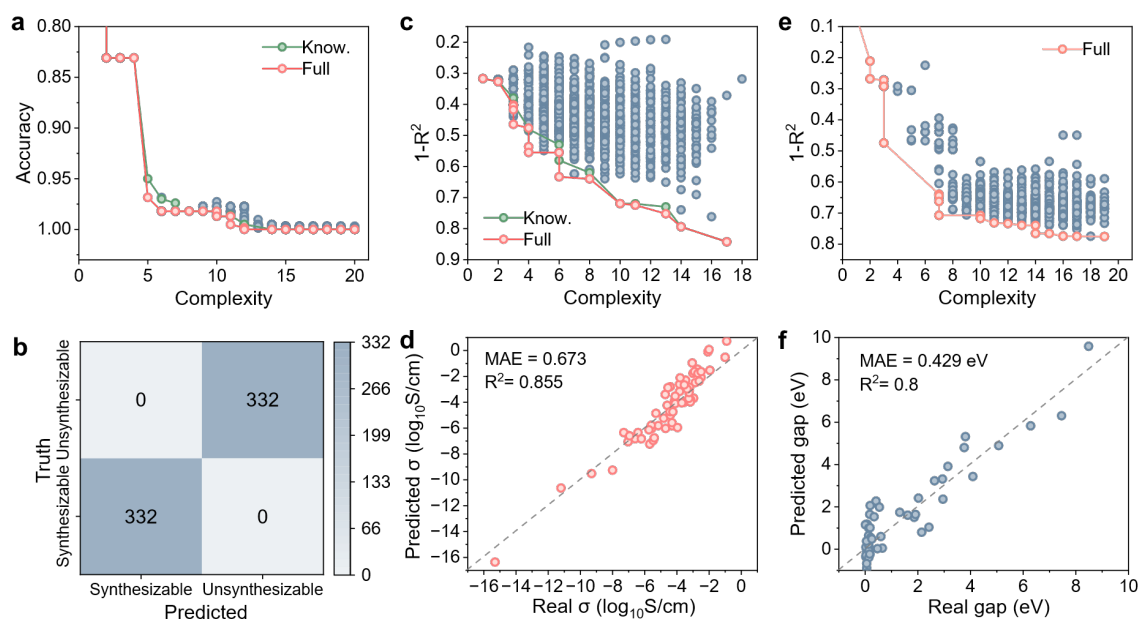


Figure 4. Performance of LLM-Feynman on additional classification and regression tasks. (a) Pareto frontier and (b) classification confusion matrix for LLM-Feynman in exploring the synthesizability formula of perovskites. (c) Pareto frontier and (d) predicted vs. actual conductivity for LLM-Feynman in exploring the formula for solid-state electrolyte conductivity. (e) Pareto frontier and (f) predicted vs. actual GW bandgap for LLM-Feynman in exploring the formula for the GW bandgap of 2D materials.

The above results demonstrate that LLM-Feynman achieves excellent accuracy and interpretability in formula discovery for classification tasks. To further evaluate its

general applicability, we applied it to two regression tasks: solid-state electrolyte conductivity and the GW bandgap of 2D materials, both of which are critical properties in materials science. Solid-state electrolyte conductivity is a key factor in the development of next-generation energy storage systems, influencing the performance and stability of solid-state batteries. The GW bandgap of 2D materials determines their electronic and optical properties, playing a crucial role in applications such as transistors, photodetectors, and quantum devices.

For the solid-state electrolyte conductivity formula, we used an experimental dataset⁵¹ containing 659 data points, splitting it into training and test sets at a 9: 1 ratio. Using LLM-Feynman, we automatically computed 50 composition features, from which the optimal formula on the Pareto front (Figure 4c) for predicting $\log_{10}\sigma$ was identified as follows:

$$\sigma = C_1 \cdot (T + N_{\text{Unfilled}}^3) + (E_{g(\text{elem})} - V_{\text{Nd}})^2 - \frac{C_2}{N_{\text{Unfilled}} + E_{g(\text{elem})}^6}$$

where T , $E_{g(\text{elem})}$, V_{Nd} , and N_{Unfilled} represent the temperature, average bandgap of constituent elements, average valence electron counts of metals, and average number of unfilled electronic states, respectively. The coefficients C_1 and C_2 are 0.00403 and 11.8337, respectively. This formula shows good predictive performance with an R^2 of 0.855 and an MAE of 0.673 on the testing set (Figure 4d). According to the formula explanation in LLM-Feynman (details in Supplementary Note S5), the temperature term accounts for thermal activation, while the cubic dependence on unfilled states indicates a strong link between empty electronic orbitals and ion transport. The squared difference between the average elemental bandgap and valence electron count captures shifts in conduction pathways. The final negative fraction penalizes excessive unfilled states or large bandgaps that hinder carrier mobility. Through its precise balance of these factors, the expression predicts conductivity across varied compositions and temperatures with notable accuracy.

For the formula of the GW bandgap of 2D materials, we utilized 551 GW bandgap data points from the high-throughput calculations of Rasmussen *et al*⁵⁵. The dataset was divided into a 9:1 training-to-test ratio. LLM-Feynman identified a Pareto-optimal

formula (Figure 4e) from 45 structural component features, effectively capturing key factors influencing the GW bandgap.

$$(\text{Dist}^3 \cdot (\text{VoroMol} + \text{AtomRadPol} - \text{TetraSys}) - \text{OrthoSys})^6$$

where Dist, VoroMol, AtomRadPol, TetraSys, and OrthoSys represent the distance from clusters with an absolute prediction error ($|\text{APE}|$) less than 0.010, the Voronoi coordination number divided by molecular volume, the atomic radius divided by polarizability, a binary variable indicating whether the material adopts a tetragonal crystal system (1 if true, 0 otherwise), and a binary variable indicating whether the material adopts an orthorhombic crystal system (1 if true, 0 otherwise), respectively. This formula achieves an R^2 of 0.80 and an MAE of 0.429 on the testing set (Figure 4f) and predicts the GW bandgap of 2D materials by combining structural and electronic factors (details in Supplementary Note S6). It includes a cubic dependence on the distance from low-error clusters, enhancing the influence of favorable structural environments. Atomic packing efficiency and polarizability contributions are summed, with tetragonal symmetry acting as a subtractive adjustment. Orthorhombic symmetry imposes an additional penalty, reducing the formula value. The entire expression is raised to the sixth power, amplifying differences in structural and electronic configurations. This formulation accounts for key interactions affecting bandgap behavior, ensuring sensitivity to variations in atomic arrangement and symmetry constraints.

Table 1. Performance comparison of three feature computation methods on three tasks.

Feature computation methods	Perovskite Synthesizability Classification Test Set Accuracy	Solid-State Electrolyte Conductivity Test Set R^2	2D Material GW Bandgap Test Set R^2
LLM-suggest	100%	0.687	0.711
LLM-suggest-iterative	100%	0.709	0.715
Automatminer+MI	100%	0.855	0.800

Notably, in the three applications above, we also tested two additional LLM-based automatic feature computation methods (Table 2). The formulas derived from LLM-recommended features exhibit significantly lower performance compared to those obtained using Automatminer, where features were computed and filtered based on mutual information. Allowing the LLM to recommend new formulas when no performance improvement was observed after 50 iterations of LLM-driven optimization can slightly improve the accuracy, while the improvement is rather limited. This suggests that in materials science, LLMs have yet to replace existing feature engineering tools. Further advancements in the LLM-based feature engineering framework or improvements in LLM performance are necessary.

Conclusion

In summary, we introduce the LLM-Feynman framework, which integrates automated data preprocessing, LLM-based symbolic regression with self-evaluation and optimization, and Monte Carlo tree search for formula interpretation to automatically extract generalizable and interpretable scientific formulas from data and domain knowledge. Ablation studies demonstrate that our framework not only outperforms conventional methods such as SISSO and PySR in accuracy and complexity but also robustly rediscovered over 90% of physical formulas from Feynman physics lectures. Notably, our framework achieves exceptional performance across four pivotal tasks in materials science: for classification, it predicts the synthesizability of 2D materials and perovskite structures with accuracies exceeding 90%, while for regression, it estimates the ionic conductivity of lithium solid-state electrolytes and the GW bandgap of 2D materials with R^2 values above 0.8 on testing datasets. This performance, combined with its modular design that facilitates seamless integration with any state-of-the-art LLMs, positions our framework as a transformative tool that will continually evolve in step with advancements in LLM technology.

However, despite these advances, our framework currently faces limitations due to the inherent token-length restrictions of contemporary LLMs, which impede its application to tasks involving extremely large datasets (e.g., on the order of 10^4

samples). Addressing this bottleneck will be essential for extending the framework’s utility to large-scale problems, and future work will explore solutions such as hierarchical data processing, architectural enhancements, and the incorporation of reinforcement learning with human feedback (RLHF)⁵⁶ to effectively manage and optimize large inputs. Despite these limitations, LLM-Feynman address the lack of domain knowledge of data-driven interpretable ML method and pave the way for automated, high-fidelity scientific discovery.

3. Methods

3.1 Inferences of large language model

Three large language models, Falcon-Mamba-7B⁴¹, ChemLLM-20B⁴², and LLaMA3-8B⁴³ were employed in the LLM-Feynman framework. These models were loaded using the Transformers library, with inference accelerated by FlashAttention⁵⁷ and Accelerate library⁵⁸. We adjusted key decoding parameters, setting the temperature to 0.7, top-k to 50, and top-p to 0.9 to balance diversity and precision. Figure S2-7,9-14 shows the model prompts, designing to provide structured responses in LLM-Feynman. All the inferences were performed on a server with one NVIDIA A800 GPU with 80 GB VRAM and 1 TB memory.

3.2 Feature engineering

To automate feature engineering for materials science formula discovery, we employ Automatminer^{39,40}, a framework that integrates multiple feature generation strategies to construct an initial feature set, denoted as X_{ini} . Automatminer systematically extracts formula from composition, structure, and electronic properties, ensuring a comprehensive representation of material characteristics. Feature selection is performed via mutual information (MI), implemented using the MODNet⁵⁹ preprocessing module. Mutual information quantifies the dependence between two variables, defined as

$$I(X, Y) = \sum_{x \in X} \sum_{y \in Y} p(x, y) \log \frac{p(x, y)}{p(x)p(y)}$$

where $p(x, y)$ is the joint probability distribution, and $p(x)$, $p(y)$ are marginal distributions. MI is computed between features and the target variable to retain

informative formula, while redundant features with high MI among themselves are removed. This results in the final optimized feature set, X_{ifinal} , enhancing model interpretability and predictive performance.

3.3 MCTS explanation

In MCTS explanation based on LLM module, each tree node represents an interpretive idea proposed by the LLM, with its score determined by the Upper Confidence Bound (UCB):

$$UCB = Q + c\sqrt{\frac{\ln N_{\text{parent}}}{N_{\text{node}}}}$$

where Q is the self-evaluation score, N_{parent} and N_{node} denote the visit counts of the parent and current node, respectively, and c balances exploration and exploitation.

The module operates in four iterative stages: Selection, where nodes with the highest UCB values are chosen; Expansion, where the LLM generates refined interpretations; Self-evaluation, where the LLM scores new nodes for clarity and relevance; and Backpropagation, where scores update ancestor nodes. This synergy between MCTS and LLM enables efficient exploration of scientifically meaningful interpretations.

Acknowledgements

This work was supported by the National Key Research and Development Program of China (grant 2022YFA1503103, 2021YFA1500700), the Natural Science Foundation of China (grant 22033002, 9226111, 22373013, T2321002), and the Basic Research Program of Jiangsu Province (BK20232012, BK20222007), Jiangsu Provincial Scientific Research Center of Applied Mathematics (BK20233002) and the Fundamental Research Funds for the Central Universities. We thank the National Supercomputing Center of Tianjin and the Big Data Computing Center of Southeast University for providing the facility support on the calculations.

Conflict of Interest

The authors declare no competing interests.

Reference

1. JONES, H. S. Tycho Brahe (1546–1601)*. *Nature* **158**, 856–861 (1946).
2. Russell, J. L. Kepler’s Laws of Planetary Motion: 1609–1666. *Br. J. Hist. Sci.* **2**, 1–24 (1964).
3. Newton, I. *Philosophiæ naturalis principia mathematica*. **1**, (G. Brookman, 1833).
4. Butler, K. T., Davies, D. W., Cartwright, H., Isayev, O. & Walsh, A. Machine learning for molecular and materials science. *Nature* **559**, 547–555 (2018).
5. Zhang, Q. *et al.* Machine Learning-Aided Design of Highly Conductive Anion Exchange Membranes for Fuel Cells and Water Electrolyzers. *Adv. Mater.* **36**, 2404981 (2024).
6. Dai, Y. *et al.* Machine-Learning-Driven G-Quartet-Based Circularly Polarized Luminescence Materials. *Adv. Mater.* **36**, 2310455 (2024).
7. Lu, S. *et al.* Coupling a Crystal Graph Multilayer Descriptor to Active Learning for Rapid Discovery of 2D Ferromagnetic Semiconductors/Half-Metals/Metals. *Adv. Mater.* **32**, 2002658 (2020).
8. Lu, S., Zhou, Q., Guo, Y. & Wang, J. On-the-fly interpretable machine learning for rapid discovery of two-dimensional ferromagnets with high Curie temperature. *Chem* **8**, 769–783 (2022).
9. Weng, B. *et al.* Simple descriptor derived from symbolic regression accelerating the discovery of new perovskite catalysts. *Nat. Commun.* **11**, 3513 (2020).
10. Song, Z. *et al.* Distilling universal activity descriptors for perovskite catalysts from multiple data sources via multi-task symbolic regression. *Mater. Horizons* **10**, 1651–1660 (2023).
11. Lu, S. *et al.* Accelerated discovery of stable lead-free hybrid organic-inorganic perovskites via machine learning. *Nat. Commun.* **9**, 3405 (2018).
12. Wu, Y. *et al.* Universal machine learning aided synthesis approach of two-dimensional perovskites in a typical laboratory. *Nat. Commun.* **15**, 138 (2024).
13. Chen, X., Lu, S., Chen, Q., Zhou, Q. & Wang, J. From bulk effective mass to 2D carrier mobility accurate prediction via adversarial transfer learning. *Nat. Commun.* **15**, 5391 (2024).
14. Murdoch, W. J., Singh, C., Kumbier, K., Abbasi-Asl, R. & Yu, B. Definitions, methods, and applications in interpretable machine learning. *Proc. Natl. Acad. Sci.* **116**, 22071–22080 (2019).
15. Schmidt, M. & Lipson, H. Distilling Free-Form Natural Laws from Experimental Data. *Science* **324**, 81–85 (2009).
16. Makke, N. & Chawla, S. Interpretable scientific discovery with symbolic regression: a review. *Artif. Intell. Rev.* **57**, 2 (2024).
17. Bartel, C. J. *et al.* Physical descriptor for the Gibbs energy of inorganic crystalline solids and temperature-dependent materials chemistry. *Nat. Commun.* **9**, 4168 (2018).
18. Bartel, C. J. *et al.* New tolerance factor to predict the stability of perovskite oxides and halides. *Sci. Adv.* **5**, eaav0693 (2019).
19. Wang, T. *et al.* Nature of metal-support interaction for metal catalysts on oxide supports. *Science* **386**, 915–920 (2024).
20. Andersen, M., Levchenko, S. V., Scheffler, M. & Reuter, K. Beyond Scaling Relations for the Description of Catalytic Materials. *ACS Catal.* **9**, 2752–2759 (2019).
21. Liu, A. *et al.* Deepseek-v3 technical report. *arXiv Prepr. arXiv2412.19437* (2024).
22. Guo, D. *et al.* DeepSeek-R1: Incentivizing Reasoning Capability in LLMs via Reinforcement Learning. *arXiv Prepr. arXiv2501.12948* (2025).

23. Cao, Y. *et al.* A Comprehensive Survey of AI-Generated Content (AIGC): A History of Generative AI from GAN to ChatGPT. *arXiv:2303.04226* (2023).
24. Touvron, H. *et al.* LLaMA: Open and Efficient Foundation Language Models. *arXiv:2302.13971* (2023).
25. Ramos, M. C., Collison, C. J. & White, A. D. A review of large language models and autonomous agents in chemistry. *Chem. Sci.* (2025). doi:10.1039/D4SC03921A
26. Jablonka, K. M., Schwaller, P., Ortega-Guerrero, A. & Smit, B. Leveraging large language models for predictive chemistry. *Nat. Mach. Intell.* **6**, 161–169 (2024).
27. Boiko, D. A., MacKnight, R., Kline, B. & Gomes, G. Autonomous chemical research with large language models. *Nature* **624**, 570–578 (2023).
28. M. Bran, A. *et al.* Augmenting large language models with chemistry tools. *Nat. Mach. Intell.* **6**, 525–535 (2024).
29. Zheng, Z., Zhang, O., Borgs, C., Chayes, J. T. & Yaghi, O. M. ChatGPT Chemistry Assistant for Text Mining and the Prediction of MOF Synthesis. *J. Am. Chem. Soc.* **145**, 18048–18062 (2023).
30. Kim, S., Jung, Y. & Schrier, J. Large Language Models for Inorganic Synthesis Predictions. *J. Am. Chem. Soc.* **146**, 19654–19659 (2024).
31. Song, Z., Lu, S., Ju, M., Zhou, Q. & Wang, J. Is Large Language Model All You Need to Predict the Synthesizability and Precursors of Crystal Structures? *arXiv Prepr. arXiv2407.07016* (2024).
32. Yang, K. *et al.* LeanDojo: Theorem Proving with Retrieval-Augmented Language Models. *Adv. Neural Inf. Process. Syst.* **36**, 1–40 (2023).
33. Yu, S., Ran, N. & Liu, J. Large-language models: The game-changers for materials science research. *Artif. Intell. Chem.* **2**, 100076 (2024).
34. Shojaee, P., Meidani, K., Gupta, S., Farimani, A. B. & Reddy, C. K. LLM-SR: Scientific Equation Discovery via Programming with Large Language Models. (2024).
35. White, D. R., Yoo, S. & Singer, J. The programming game: evaluating mcts as an alternative to gp for symbolic regression. in *Proceedings of the Companion Publication of the 2015 Annual Conference on Genetic and Evolutionary Computation* 1521–1522 (2015). doi:10.1145/2739482.2764655
36. Ouyang, R., Ahmetcik, E., Carbogno, C., Scheffler, M. & Ghiringhelli, L. M. Simultaneous learning of several materials properties from incomplete databases with multi-task SISSO. *J. Phys. Mater.* **2**, 024002 (2019).
37. Ouyang, R., Curtarolo, S., Ahmetcik, E., Scheffler, M. & Ghiringhelli, L. M. SISSO: A compressed-sensing method for identifying the best low-dimensional descriptor in an immensity of offered candidates. *Phys. Rev. Mater.* **2**, 83802 (2018).
38. Cranmer, M. Interpretable Machine Learning for Science with PySR and SymbolicRegression.jl. (2023).
39. Ward, L. *et al.* Matminer: An open source toolkit for materials data mining. *Comput. Mater. Sci.* **152**, 60–69 (2018).
40. Dunn, A., Wang, Q., Ganose, A., Dopp, D. & Jain, A. Benchmarking materials property prediction methods: the Matbench test set and Automatminer reference algorithm. *npj Comput. Mater.* **6**, 138 (2020).
41. Gu, A. & Dao, T. Mamba: Linear-Time Sequence Modeling with Selective State Spaces. *arXiv preprint arXiv:2312.00752* (2023).
42. Zhang, D. *et al.* ChemLLM: A Chemical Large Language Model. (2024).

43. Llama Team, A. The Llama 3 Herd of Models. *arXiv:2407.21783* (2024).
44. Udrescu, S.-M. & Tegmark, M. AI Feynman: A physics-inspired method for symbolic regression. *Sci. Adv.* **6**, eaay2631 (2020).
45. Hastrup, S. *et al.* The Computational 2D Materials Database: High-throughput modeling and discovery of atomically thin crystals. *2D Mater.* **5**, 042002 (2018).
46. Campi, D., Mounet, N., Gibertini, M., Pizzi, G. & Marzari, N. Expansion of the Materials Cloud 2D Database. *ACS Nano* **17**, 11268–11278 (2023).
47. Mounet, N. *et al.* Two-dimensional materials from high-throughput computational exfoliation of experimentally known compounds. *Nat. Nanotechnol.* **13**, 246–252 (2018).
48. Tang, C. *et al.* Energy-Saving Electrolytic Hydrogen Generation: Ni 2 P Nanoarray as a High-Performance Non-Noble-Metal Electrocatalyst. *Angew. Chemie* **129**, 860–864 (2017).
49. Hellenbrandt, M. The inorganic crystal structure database (ICSD) - Present and future. *Crystallogr. Rev.* **10**, 17–22 (2004).
50. Jang, J., Gu, G. H., Noh, J., Kim, J. & Jung, Y. Structure-Based Synthesizability Prediction of Crystals Using Partially Supervised Learning. *J. Am. Chem. Soc.* **142**, 18836–18843 (2020).
51. Xie, T. & Grossman, J. C. Crystal Graph Convolutional Neural Networks for an Accurate and Interpretable Prediction of Material Properties. *Phys. Rev. Lett.* **120**, 145301 (2018).
52. Finn, C., Abbeel, P. & Levine, S. Model-agnostic meta-learning for fast adaptation of deep networks. in *International conference on machine learning* 1126–1135 (2017).
53. Jain, A. *et al.* Commentary: The Materials Project: A materials genome approach to accelerating materials innovation. *APL Mater.* **1**, 011002 (2013).
54. Kirklin, S. *et al.* The Open Quantum Materials Database (OQMD): assessing the accuracy of DFT formation energies. *npj Comput. Mater.* **1**, 15010 (2015).
55. Rasmussen, A., Deilmann, T. & Thygesen, K. S. Towards fully automated GW band structure calculations: What we can learn from 60.000 self-energy evaluations. *npj Comput. Mater.* **7**, 22 (2021).
56. Kirk, R. *et al.* Understanding the Effects of RLHF on LLM Generalisation and Diversity. in *12th International Conference on Learning Representations (ICLR, 2024)*.
57. Dao, T. FlashAttention-2: Faster Attention with Better Parallelism and Work Partitioning. in *12th International Conference on Learning Representations (ICLR, 2024)*.
58. Gugger, S. *et al.* Accelerate: Training and inference at scale made simple, efficient and adaptable. (2022).
59. De Breuck, P.-P., Hautier, G. & Rignanese, G.-M. Materials property prediction for limited datasets enabled by feature selection and joint learning with MODNet. *npj Comput. Mater.* **7**, 83 (2021).

